ChemComm

Effects of Sidechain Isomerism on Polymer-based Non-Covalent Protein Delivery

Journal:	*ChemComm*
Manuscript ID	CC-COM-04-2022-002343.R1
Article Type:	Communication

COMMUNICATION

Effects of Sidechain Isomerism on Polymer-based Non-Covalent Protein Delivery

Received 00th January 20xx,
Accepted 00th January 20xx

DOI: 10.1039/x0xx00000x

Alfonso Barrios,[a] Mario Milan Diaz,[a] Elianny Perozo,[a] Md Lokman Hossen,[b] Prem Chapagain,[b,c] and Joong Ho Moon*[a,c]

We present the importance of functional group isomerism on intracellular protein delivery using polymers containing different isomeric side chains. While the physical properties of polymer/protein complexes are relatively similar, different planarity of the isomers greatly influences the cellular entry efficiency.

Protein-based therapeutics have gained much recent attention for treating or curing various diseases. Their therapeutic success is due to high specificity, low side effects, less immunogenicity, and relatively short regulatory approval time than small molecular drugs.[1] Despite their advantages, the cell impermeability of most proteins has limited their applications to extracellular targets.[2] As more than 60% of intracellular protein signaling pathways control cellular functions, the intervention of disease-causing or -related signaling pathways would contribute to treating various diseases, including traditionally uncurable diseases using molecular drugs.[1,3–5] Therefore, there have been extensive efforts to develop efficient intracellular protein delivery systems.

Polymer-based non-covalent protein delivery systems have gained significant attention owing to the versatile tunability of the functional groups, compositions, and architectures.[6–8] Numerous structural (i.e., backbones) and functional groups (i.e., sidechains) for ionic, hydrogen bonding (HB), and hydrophobic interactions have been developed for facile protein complexation, cellular entry, and cytosolic release of functional proteins. The efficient protein delivery critically relies on optimized and balanced inter-macromolecular interactions. Without sufficient protein binding affinity, a premature dissociation of the complex occurs in the presence of excess serum proteins and upon interaction with the cellular membranes.[9,10] With excessively high affinity, structural deformations and retarded desorption of polymers from the protein surface result in decreased concentrations of active proteins in the cytosol.[11]

Both structural and functional groups collectively influence the interactions with lipid membranes and entry pathways during cellular entry. While differences in cellular uptakes arising from tailored polymer backbone architecture have been reported,[12–14] little is known about the effects of subtle differences in the functional groups' conformation, isomerism, rigidity, and planarity. Most recently, Johnson et al. reported polymers with enantiomeric side chains displaying changed cellular uptakes and pharmacokinetic properties due to their different chiral recognition.[15] Our group also observed significant changes in the protein delivery efficiency from modified guanidine groups. Using various carbamoylated guanidine (CG) derivatives, we demonstrated the importance of the newly developed functional group for complex serum stability, cellular entry, and cytosolic availability of proteins.[16] While CG derivatives benefited from enhanced serum stability, the direct attachment of the phenyl group to CG contributed most to efficient protein delivery, presumably due to its planar structure. CG derivatives lacking planarity due to free rotating benzyl groups exhibited poor protein delivery, prompting us to explore how these subtle changes govern biological functions.

Herein, we report the effects of the constitutional isomerism of the Ph-CG group on functional protein delivery (Figure 1). From the backbone of polynorbornene (PN), the order of connectivity in phenyl-CG (Ph-CG) was altered to make an isomeric Ph-CG'. An isomer (Bn-CG') of benzyl-CG (Bn-CG) was also tested to expand the concept of the isomer effect. Molecular dynamics simulations reveal that the isomeric functional group (i.e., Ph-CG') has a non-planar structure with less rotational freedom along the bond between nitrogen and sp^2 carbon in the phenyl group, while Ph-CG exhibits the

[a] *Department of Chemistry and Biochemistry, Florida International University, 11200 SW 8th St., Miami, FL 33199, USA.*
[b] *Department of Physics, Florida International University, 11200 SW 8th St., Miami, FL 33199, USA*
[c] *Biomolecular Sciences Institute, Florida International University, 11200 SW 8th St., Miami, FL 33199, USA*
† Footnotes relating to the title and/or authors should appear here.
Electronic Supplementary Information (ESI) available: Detailed methods, polymer characterization, and additional data. See DOI: 10.1039/x0xx00000x

planarity. Strikingly, while the complex sizes, protein loading, and serum stability are not significantly affected by the different

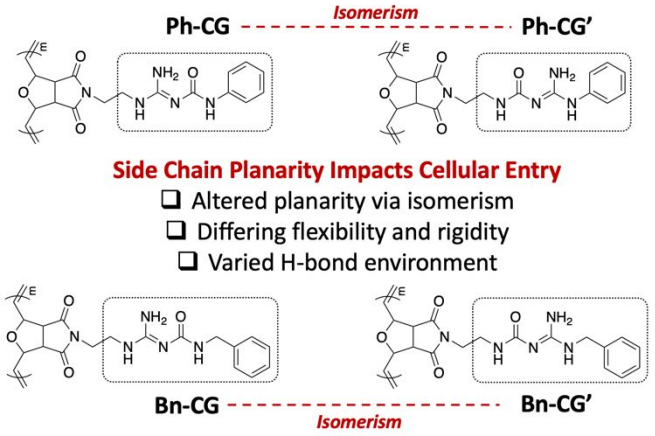

Figure 1. Chemical structures of polymers. Ph: Phenyl, Bn: Benzyl, CG: Carbamoylated Guanidine. Isomers are denoted with a prime (i.e.,') for simplicity.

planarity of the isomers, the cellular entry of the resulting complex and intracellular protein activities were significantly influenced by the connectivity. This approach demonstrates the importance of a key structural component of polymeric carriers required for highly efficient functional intracellular protein delivery.

Previously reported polynorbornes (PNs)-containing Ph-CG and Bn-CG, respectively, were used to study the effects of the functional group isomerism. In the case of Ph-CG' and Bn-CG', the respective monomers were prepared and polymerized (Scheme S1), leading to the pairs of constitutional isomers (Figure 1).

Molecular dynamics simulations were performed to investigate the flexibility and planarity of the isomeric functional groups in the side chains. The dihedral angles ϕ and ψ, as defined in Figure 2, were calculated. The dynamics of the bonds are given by the fluctuations in the measured dihedral angles as a function of the simulation time. As shown in Figure S1, Ph-CG shows high rotational flexibility along the sp^2 C-N bond, whereas the dihedrals of Ph-CG' are much more restricted and show less rotational flexibility. Although there is fast rotation, the Ph group in Ph-CG is mostly populated in conformations at the combinations of ϕ and ψ in the range of (0, ±180) and (±180, ±180), indicating higher planarity of Ph-CG. In contrast, the combinations of ϕ and ψ for Ph-CG' are close to ±90 and ±90, respectively, indicating the phenyl group is perpendicular (i.e., bent) to guanidine. It has been reported that the steric hindrance arising between the aryl and amine protons in Ph-CG' leads to a non-planar conformation.[17]

Complexation with cargo proteins was achieved by mixing a PN solution in water containing a low percentage of dimethylsulfoxide (DMSO) and corresponding protein with different sizes and isoelectric points (pIs) in phosphate-buffered saline (PBS). Despite the broad size differences in proteins, all polymer-protein complexes exhibit similar hydrodynamic diameters (HDs) and zeta potentials (ζ), except Bn-CG showing relatively small HD (Table 1, Table S1, and Figure S2). Similarly, the pK_a values of the isomeric functional groups were

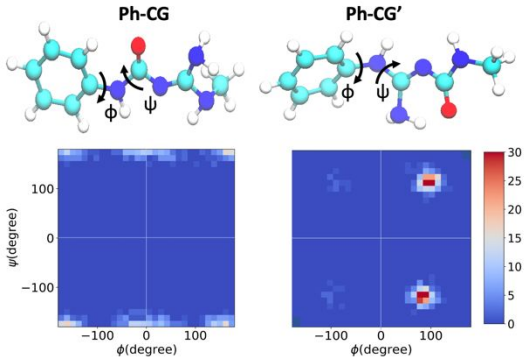

Figure 2. Conformational flexibility of polymer isomers. Structures of the compounds Ph-CG and Ph-CG' showing the dihedral angles (ϕ and ψ) and 2D histograms of the dihedral angles ϕ and ψ of the compounds. The color bar shows the frequency (%) of structures that occur during the simulation.

Table 1. Summary of physical characterization for PNs and PN/R-PE complexes.

PNs	M_n[a]	M_w[a]	pK_a[a]	HD[b]	ζ[c]	K_d[d]
Ph-CG	5.5	5.9	6.1	194 ± 49	-10.2 ± 0.8	219 ± 42
Bn-CG	5.7	6.1	6.1	159 ± 55	-6.0 ± 2.6	234 ± 37
Ph-CG'	5.8	6.4	5.4	212 ± 55	-5.2 ± 0.3	341 ± 51
Bn-CG'	6.1	7.0	6.0	210 ± 46	-7.4 ± 3.3	143 ± 27

[a] Molecular weights (M_n and M_w, kDa) and acidity constant (pK_a) of PNs. [b] Hydrodynamic diameters (HD, nm) of PN/R-PE complexes (10 μM/10 μg/mL). Values represent mean ± standard deviation of the arithmetic values calculated for all nanoparticles recorded by the NTA software. [c] Zeta potentials (mV) of PN/R-PE complexes in DPBS (345 μM NaCl), where R-PE is 0.625 μg/mL). [d] Dissociation constant (K_d, nM) of PN/R-PE complexes.

measured to be between 5.4 and 6.1. Notably, Ph-CG' exhibited a lower pK_a of 5.4, presumably due to the resonance contribution of the adjacent phenyl ring next to the protonatable group. Acylation in guanidine has been reported and used to tune the pK_a of guanidine-containing small molecules.[18,19] Through conjugation of the electron-withdrawing acyl group, the pKa of acyl guanidine was reported to be ~8.[19] Previously, we also reported that the carbamoylation of guanidine led to a sharp pK_a decrease in guanidine.[16] All CG-containing PNs exhibit a charge-neutral state in the physiological environment. Despite the lack of positive charge, synergistic HB and hydrophobic interactions have been reported as the major driving forces for non-ionic protein complexation.[10,20–22] With the increased number of HB donors, the hydrophobic aromatic group introduced at the close vicinity of CG is believed to favorably contribute to stable complex formation. Calculation of K_d for PN/protein complexes indicates that the binding affinity of PNs to fluorescent proteins (FPs) with different sizes is in a nanomolar concentration range (Table 1, Figure S3, and Table S2). The protein loading efficiency in the complex was estimated by measuring the amounts of free FPs in the supernatant after centrifugation of complexes. Regardless of the protein sizes, all PNs show similar high protein loading efficiency at the concentration used for cellular delivery (i.e., above 2.5 μM) (Figure S4). Lastly, the complex stability in PBS containing 10% fetal bovine serum (FBS) was also very similar among the isomers (Figure S5). Overall, all the HDs, ζ,

protein loading efficiency, K_d, and complex serum stability data indicate that the protein complexation behaviors of CG-containing PNs, regardless of the isomerism and planarity, are similar due to the CG group enhancing the inter-macromolecular interactions. All PNs exhibit no cell viability inhibition on HeLa cells at the concentrations tested (Figure S6).

While the physical properties of the complexes are similar, the cellular protein delivery efficiency of PNs, measured by flow cytometry, is quite different. The mean fluorescent intensity (MFI) of HeLa cells treated with PN/R-PE complex formed at various PN to R-PE ratios was monitored to study the optimum formulation yielding the highest intracellular R-PE concentration (Figure S7). R-PE is a red fluorescent protein isolated from red algae and used as a model protein for cellular delivery. The membrane adsorbed R-PE fluorescence signals were quenched by treating with trypan blue (TB) (see below discussion without TB treatment). As shown in Figure 3, Ph-CG has a higher MFI (i.e., four folds) and percent R-PE positive cells than Ph-CG', its constitutional isomer. Considering the similar complex size, serum stability, and loading efficiency, the differences observed can be attributed to different cellular entry abilities of the complex, presumably due to the planarity of Ph-CG. The non-planar and bent conformation of Ph-CG' could be tied with the decreased cellular interactions and/or internalization, resulting in low protein delivery ability. A similar trend was also observed between Bn-CG and Bn-CG', in which Bn-CG shows a 2-fold higher MFI than Bn-CG'. From the different cellular delivery efficiencies between Bn-CG and Bn-CG', in which both functional groups have no coplanarity with the Bn group due to the free-rotating methylene spacers, the isomeric relationship of Bn-CG and Bn-CG' also influences cellular delivery. The concentrations of internalized proteins were gradually increased as the incubation time increased (Figure S8), and similar delivery efficiency of R-PE to different cell types was also observed (Figure S9).

Considering the similar physical properties of complex, the substantial differences in the R-PE internalization efficacy are pretty interesting. To examine the degree of internalized protein and protein adsorbed on the membranes, the MFI of HeLa cells with and without TB treatment was measured.[20]

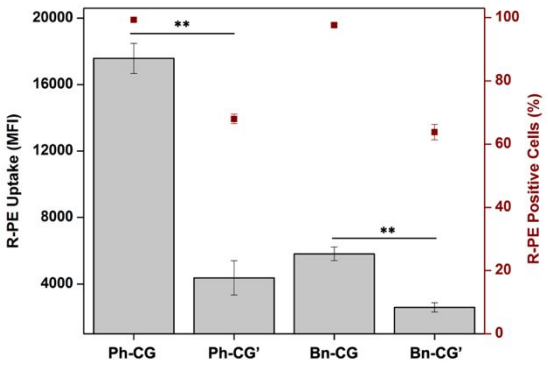

Figure 3. MFI and percent positive cells of HeLa cells treated with PN/R-PE complexes for 18 h. The concentrations of polymer and R-PE were 2.5 μM and 0.5 μg/mL, respectively. Membrane adsorbed R-PE signal was quenched with TB. Data shown are the mean of three independent experiments ± standard deviation. ** $p<0.01$.

Before the TB treatment, the complex-treated cells were thoroughly rinsed with PBS (three times) and a heparin sulfate solution. As shown in Figure S10, both Ph-CG and Ph-CG' demonstrate relatively similar MFI without the TB treatment at 5 μM of PNs. However, while Ph-CG only shows a ~2-fold decrease in fluorescence quenching upon TB treatment, the isomer Ph-CG' has ~5-fold decreased MFI. Assuming the similar colloidal stability of the complexes (i.e., a similar range of ζ), this observation implies that initial membrane interactions of Ph-CG/R-PE and Ph-CG' could be similar at the same complexation ratio (i.e., 5 μM PN/0.5 μg/ml R-PE) (i.e., similar fluorescent intensity before the TB treatment). However, when the fluorescent intensity from the membrane adsorbed PN/R-PE complex was quenched, the higher internalized R-PE signals imply that Ph-CG with planarity internalizes R-PE more efficiently than non-planar Ph-CG'. Interestingly, the proportions of internalized R-PE after TB treatment were also decreased when excess amounts of PNs were used (Figure S10), which could be due to poor aqueous solubility of PNs causing/contributing aggregations and/or reducing the proportion of the PN/protein complex interacting the cell membranes, implying that there might be an optimum PN concentration needed for facilitating the internalization process.

Cellular entry pathway studies demonstrate that the internalization of R-PE by both Ph-CG and Ph-CG' primarily occurs via energy-dependent pathways, as the treatment at 4 °C and ATP-depleted conditions significantly decrease the uptakes. Pretreatment with various chemical endocytosis inhibitors implies that macropinocytosis is the primary entry pathway along with other pathways. There are negligible differences in the inhibition pattern between both isomeric carriers (Figure S11). As revealed by the confocal images in Figure S12, FITC-BSA delivered by Ph-CG is dispersed inside the cell, within the boundaries of the membrane stained with Actin Red, while Ph-CG' exhibits almost no green signals under the same incubation condition. To determine whether FITC-BSA delivered by Ph-CG and Ph-CG', respectively, is located in the endosome/lysosome, a counter-staining was done with Lysotracker Red, and Pearson's correlation coefficient (PCC) scorning was conducted to quantitatively analyze the overlap between two colors. As seen in Figure S13, PCC values of 0.356 and 0.128 were found for Ph-CG and Ph-CG', respectively. The higher PCC value for Ph-CG is likely due to significantly higher green signals from the delivered FITC-BSA than Ph-CG', and not necessarily due to higher endosomal entrapment.

Maintaining the structure and function of the complexed and delivered proteins is crucial in the development of protein carriers. A large enzyme, β-Galactocidase (β-Gal), was intracellularly delivered by Ph-CG. Generation of blue color in the cells upon treatment of the enzyme-substrate 5-bromo-4-chloro-3-indolyl β-D-galactopyranoside (X-Gal) indicates that the delivered proteins maintain their enzymatic activities.[23] As seen in Figure 4a, cells treated with Ph-CG/β-Gal complexes demonstrate a clear blue color compared to controls. We further tested the efficacy in functional protein delivery using an anti-apoptotic antibody, anti-pAkt. Protein kinase B (Akt) is

involved in cellular survival pathways by inhibiting apoptotic processes. Therefore, blocking the pathway inhibits cell growth and proliferation.[23,24] While the cell membrane-impermeable antibody alone shows negligible cell viability inhibition, an exponential decrease in viability was observed when anti-pAkt was delivered by Ph-CG. The isomeric Ph-CG' mediated delivery also exhibits a decrease in viability but has relatively poor

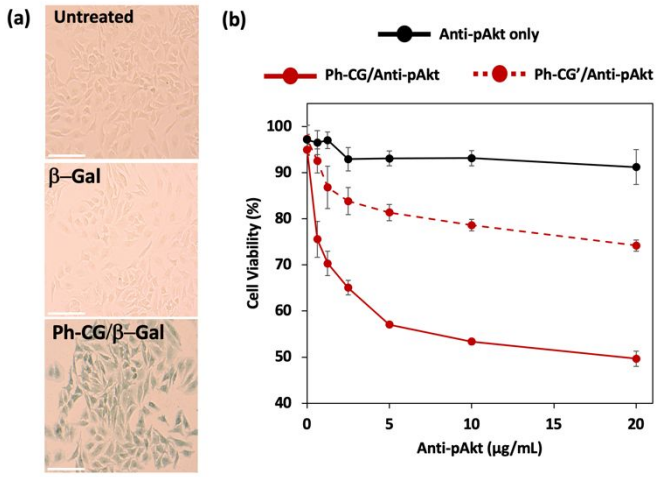

Figure 4. (a) X-Gal staining of treated HeLa cells. Final concentrations of Ph-CG and β-Gal were 2.5 μM and 0.5 μg/mL. Untreated cells and β-Gal alone are shown as controls. Scale bar: 150 μm (b) Viability of HeLa cells treated with PN/anti-pAkt complexes or anti-pAkt alone at various antibody concentrations. The concentration of PN was kept constant at 10 μM. Data represent the mean ± standard deviation.

activity (Figure 4b). The cell viability inhibition results support that the delivered antibody maintains its activity and reaches its epitope in the cytosol. The functional antibody delivery also confirmed the difference in the intracellular entry efficiency between the isomeric complexes.

In conclusion, we report a dramatic influence of the functional group isomerism on intracellular protein delivery. Remarkable differences were observed in terms of rigidity, planarity, and ultimately protein delivery behavior for pairs of polymers with isomeric side chains. While electrostatic, hydrogen bonding, and hydrophobic inter-macromolecular interactions are relatively similar in the tested polymers, the PN containing a planar Ph-CG moiety demonstrated significantly improved cellular entry and protein delivery ability. Overall, this work establishes the importance of rigidity, planarity, and conformation as parameters of the functional group for designing protein delivery carriers. Studying the entry efficiency and mechanism of fluorescently-labeled PN-containing different isomeric side chains should also provide useful insights into how the carriers interact with proteins and membranes. To the best of our knowledge, this is the first report on the effect of polymer side chain isomerism on protein delivery.

This work was supported by the NSF (DMR 2105016).

Conflicts of interest

There are no conflicts to declare.

Notes and references

1 Q. J. B. and D. E. G. Benjamin Leader, *Nat. Rev. Drug Discov.*, 2008, **7**, 21–39.
2 A. Fu, R. Tang, J. Hardie, M. E. Farkas and V. M. Rotello, *Bioconjug. Chem.*, 2014, **25**, 1602–1608.
3 P. J. Carter and G. A. Lazar, *Nat. Rev. Drug Discov.*, 2018, **17**, 197–223.
4 T. A. Slastnikova, A. V. Ulasov, A. A. Rosenkranz and A. S. Sobolev, *Front. Pharmacol.*, 2018, **9**, 1–21.
5 M. Diehn, R. Bhattacharya, D. Botstein and P. O. Brown, *PLoS Genet.*, 2006, **2**, 39–50.
6 A. Fu, R. Tang, J. Hardie, M. E. Farkas and V. M. Rotello, *Bioconjug. Chem.*, 2014, **25**, 1602–1608.
7 J. Lv, Q. Fan, H. Wang and Y. Cheng, *Biomaterials*, 2019, **218**, 119358.
8 X. Qin, C. Yu, J. Wei, L. Li, C. Zhang, Q. Wu, J. Liu, S. Q. Yao and W. Huang, *Adv. Mater.*, 2019, **31**, 1–32.
9 C. M. Backlund, C. R. Hango, L. M. Minter and G. N. Tew, *ACS Appl. Bio Mater.*, 2020, **3**, 180–185.
10 H. C. Davis, N. D. Posey and G. N. Tew, *Biomacromolecules*, 2022, **23**, 57–66.
11 C. R. Hango, C. M. Backlund, H. C. Davis, N. D. Posey, L. M. Minter and G. N. Tew, *Biomacromolecules*, 2021, **22**, 2850–2863.
12 G. Lättig-Tünnemann, M. Prinz, D. Hoffmann, J. Behlke, C. Palm-Apergi, I. Morano, H. D. Herce and M. C. Cardoso, *Nat. Commun.*, 2011, **2**, 453.
13 J. Sun, L. Zhang, J. Wang, Q. Feng, D. Liu, Q. Yin, D. Xu, Y. Wei, B. Ding, X. Shi and X. Jiang, *Adv. Mater.*, 2015, **27**, 1402–1407.
14 J. A. Kretzmann, D. C. Luther, C. W. Evans, T. Jeon, W. Jerome, S. Gopalakrishnan, Y. W. Lee, M. Norret, K. S. Iyer and V. M. Rotello, *J. Am. Chem. Soc.*, 2021, **143**, 4758-4765.
15 H. V. T. Nguyen, Y. Jiang, S. Mohapatra, W. Wang, J. C. Barnes, N. J. Oldenhuis, K. K. Chen, S. Axelrod, Z. Huang, Q. Chen, M. R. Golder, K. Young, D. Suvlu, Y. Shen, A. P. Willard, M. J. A. Hore, R. Gómez-Bombarelli and J. A. Johnson, *Nat. Chem.*, 2022, **14**, 85-93.
16 A. Barrios, M. Estrada and J. H. Moon, *Angew. Chemie Int. Ed.*, 2022, **61**, e202116722.
17 B. Kelly, M. McMullan, C. Muguruza, J. E. Ortega, J. J. Meana, L. F. Callado and I. Rozas, *J. Med. Chem.*, 2015, **58**, 963–977.
18 R. Kleinmaier, M. Keller, P. Igel, A. Buschauer and R. M. Gschwind, *J. Am. Chem. Soc.*, 2010, **132**, 11223–11233.
19 C. Dardonville, B. A. Caine, M. Navarro De La Fuente, G. Martín Herranz, B. Corrales Mariblanca and P. L. A. Popelier, *New J. Chem.*, 2017, **41**, 11016–11028.
20 M. Wang, H. Liu, L. Li and Y. Cheng, *Nat. Commun.*, 2014, **5**, 1–8.
21 M. Li, S. Schlesiger, S. K. Knauer and C. Schmuck, *Angew. Chemie - Int. Ed.*, 2015, **54**, 2941–2944.
22 J. Hatai and C. Schmuck, *Acc. Chem. Res.*, 2019, **52**, 1709–1720.
23 K. Dutta, P. Kanjilal, R. Das and S. Thayumanavan, *Angew. Chemie - Int. Ed.*, 2021, **60**, 1821–1830.
24 R. Liu, Y. Chen, G. Liu, C. Li, Y. Song, Z. Cao, W. Li, J. Hu, C. Lu and Y. Liu, *Cell Death Dis.*, 2020, **11**, 797.